Diamond nanocrystal thin films: Case study on surface texture and power spectral density properties

Cite as: AIP Advances 10, 045206 (2020); doi: 10.1063/5.0003866
Submitted: 11 February 2020 • Accepted: 16 March 2020 •
Published Online: 3 April 2020

Shahram Solaymani,[1] Ştefan Ţălu,[2] Negin Beryani Nezafat,[3] Sahar Rezaee,[4,a)] and Mahboubeh Fathi Kenari[5]

AFFILIATIONS

[1]Department of Physics, Harsin Branch, Islamic Azad University, 6731994934 Harsin, Iran
[2]The Directorate of Research, Development and Innovation Management (DMCDI), Technical University of Cluj-Napoca, Constantin Daicoviciu St., No. 15, Cluj-Napoca 400020, Cluj County, Romania
[3]School of Physics, Institute for Research in Fundamental Sciences (IPM), P.O. Box 19395-5531, Tehran, Iran
[4]Department of Physics, Kermanshah Branch, Islamic Azad University, 6718997551 Kermanshah, Iran
[5]Department of Physics, University of Pretoria, 0002 Pretoria, South Africa

[a)]**Author to whom correspondence should be addressed:** saharrezaee593@iauksh.ac.ir. **Permanent address**: Department of Physics, Kermanshah Branch, Islamic Azad University, Kermanshah, Iran. **Tel:** +989183333568

ABSTRACT

Analyzing diamond nanocrystal (DNC) thin film morphology produced by the HFCVD technique is the main objective of the present work. Stereometric analysis of three-dimensional surface microtextures was carried out based on data obtained through atomic force microscopy (AFM), while the ISO 25178-2:2012 standard was applied to characterize surface topography. The Abbott–Firestone curve, peak count histograms, and Cartesian graphs, which were extracted through AFM images, gave valuable statistical information. As can be seen, the most isotropic sample was the Au catalyst (etched) deposited by the hot filament chemical vapor deposition method. Moreover, by increasing the time of DNC growth from 15 min to 60 min, the surface roughness was increased. In addition, the average power spectral density was calculated and furrows were determined for all samples.

I. INTRODUCTION

The unique properties of nano-materials make them suitable candidates to be applied in various types of technologies in the field of science, biology, and engineering.[1–5] Among these types of materials, diamond nanocrystal (DNCs) thin films, because of their significant properties, motivated scientists to use them in industrial sectors over the last few decades.[5–7] Diamonds, because of their high surface to volume ratio and significant properties like high breakdown field strength, high electron and hole motilities, and large bandgap (5.5 eV), attract as much research interest as other carbon allotropes, i.e., graphite and carbon nanotubes.[8] It is the hardest material that has ever been known with the maximum value of wear resistance.

In the process of producing DNCs, several methods such as the electrochemical method, conformal coatings for micro-electro-mechanical systems (MEMSs), and the chemical vapor deposition (CVD) method have been introduced.[9–11] Between them, the chemical vapor deposition (CVD) method is considered the best method for the growth of diamond films. Hot filament CVD (HFCVD) has been used here for the growth of DNC films due to its high efficiency and low cost.[12]

Other methods require optimization of diamond properties including surface smoothness, field emission, and electrical

TABLE I. The details of the prepared samples.

Sample ID no.	Gas type	Gas flow (sccm)	Filament temperature (°C)	Substrate temperature (°C)	Time (min)	Deposition method	Yield
1	Ar	...	...	Room temperature	20	DC-magnetron sputtering	Au catalyst
2	H_2	100	1700	550	15	HFCVD	Au catalyst (etched)
3	CH_4/H_2	100	1800	600	15	HFCVD	DNCs
4	CH_4/H_2	100	1800	600	30	HFCVD	DNCs
5	CH_4/H_2	100	1800	600	60	HFCVD	DNCs

conductivity on the microscale; however, in the CVD method, the diamond film microstructure and crystalline size can be controlled in the nanoscale.

Recently, much research has been focused on the tribology of major applications of DNC films by focusing on their friction coefficients, wear rates, and hardness,[13–16] but morphological studies of these films and their surface engineering are missing.

In order to investigate surface topography of these types of materials, atomic force microscopy (AFM) has been considered as the best tool in the modern surface-imaging area.[16,17] Three-dimensional (3D) images of thin film surfaces at the microscopic level give valuable information about energy dissipation mechanisms and macroscopic friction. It should be noted that the geometry of DNCs can be extracted through AFM images by fractal[18–20] and multifractal[21,22] geometry. AFM has been applied to elucidate the surface geometry microtexture with high nanoscale resolution.[23,24] Furthermore, stereometric, fractal/multifractal analyses, as well as analyses by power spectral density (PSD) functions, are accurate tools for characterization of the nano-scale patterns in 3D complex surfaces of thin films.[25,26]

Here, we report the growth of nanocrystalline diamond thin films and study their 3D micromorphology prepared by using the HFCVD method. The fundamental properties of these films have been comprehensively investigated by AFM. Fractal/multifractal geometry along with statistical surface parameters was extracted from AFM images in order to obtain morphological information.

II. MATERIALS AND METHODS

A. Experimental details

Here, p-type Si wafers with (100) orientation were considered as the substrate, and Au was applied as the catalyst for Au thin film deposition. During the 15 min etching process of Au thin films by the HFCVD method, the working pressure and flow rate were 6.6×10^2 Pa and 100 sccm, respectively, for H_2. The filament and substrate temperatures were 1700 °C and 550 °C, respectively. It should be noted that no common surface pre-treatment was used for increasing the nucleation density of diamond nanocrystals (DNCs).[27]

Thereafter, nanostructured carbon was grown on the Au thin film. The ratio of CH_4/H_2 was set in the rate of 8%, while other mentioned parameters of the etching process were unchanged, except the filament and substrate temperatures which increased to 1800 °C and 600 °C, respectively. Growing DNCs were carried out for 15 min, 30 min, and 60 min at room temperature (297 ± 1 K). The details of each sample are summarized in Table I.

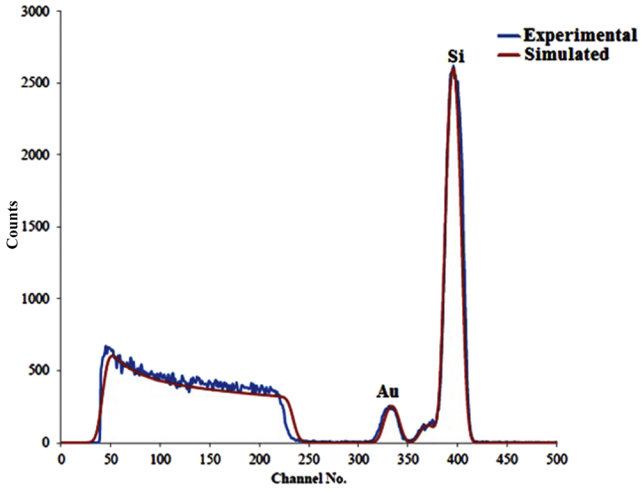

FIG. 1. Rutherford back scattering of the Au catalyst.

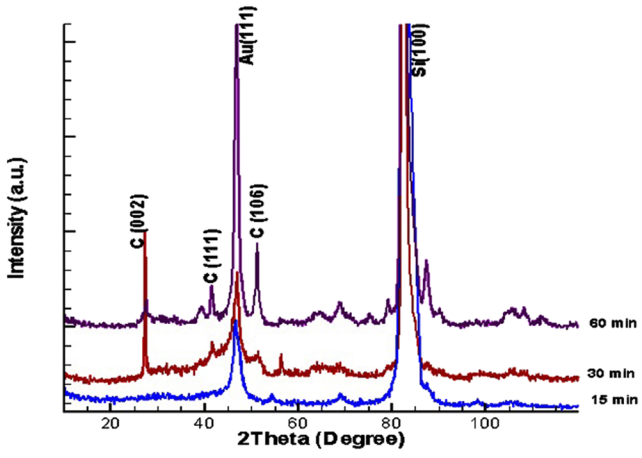

FIG. 2. XRD patterns of grown DNCs on the Au catalyst.

Here, 2.0 MeV He+ ions were produced by a van de Graff accelerator to analyze the ion beam. Solid state detectors with 15 keV resolution were located at 162° for detecting the backscattered particle. The accelerator was located at Centro de Microanalisis de Materiales (CMAM). The angle between the surface and the incident ion beam was 90°, and scattered ions with a dose of 10 mC were detected at 165° by a mobile detector. The information about the atomic content and thickness of the thin films were obtained from Rutherford backscattering (RBS) analysis using SIMN RA software.

In addition, x-ray diffraction (XRD) with Cu-kα radiation (λ = 1.54 A) was applied to record the crystalline structure of DNC samples, where 2Θ was from 0° to 100°. Atomic force microscopy (AFM) (Veeco, Santa Barbara, CA) results were finally applied to provide quantitative data on surface roughness and morphology for studying the structural topography of samples. The experiments were carried out by cantilevers with the following specific properties for force–distance curve measurements: width 25 μm, length 180 μm, thickness 4 μm, quality factor Q = 100, tip radius 10 nm, Young's modulus E = 1.3 × 10^{11} Pa, mass density ρ = 2330 kg/m^3, and Poisson's ratio ν = 0.28.[28] The 3D surface topography of thin films was investigated through 256 × 256 pixel images recorded by a non-contact mode nanoscope multimode atomic force microscope (Digital Instruments, Santa Barbara, CA) with a scan speed of 10–20 μm/s.

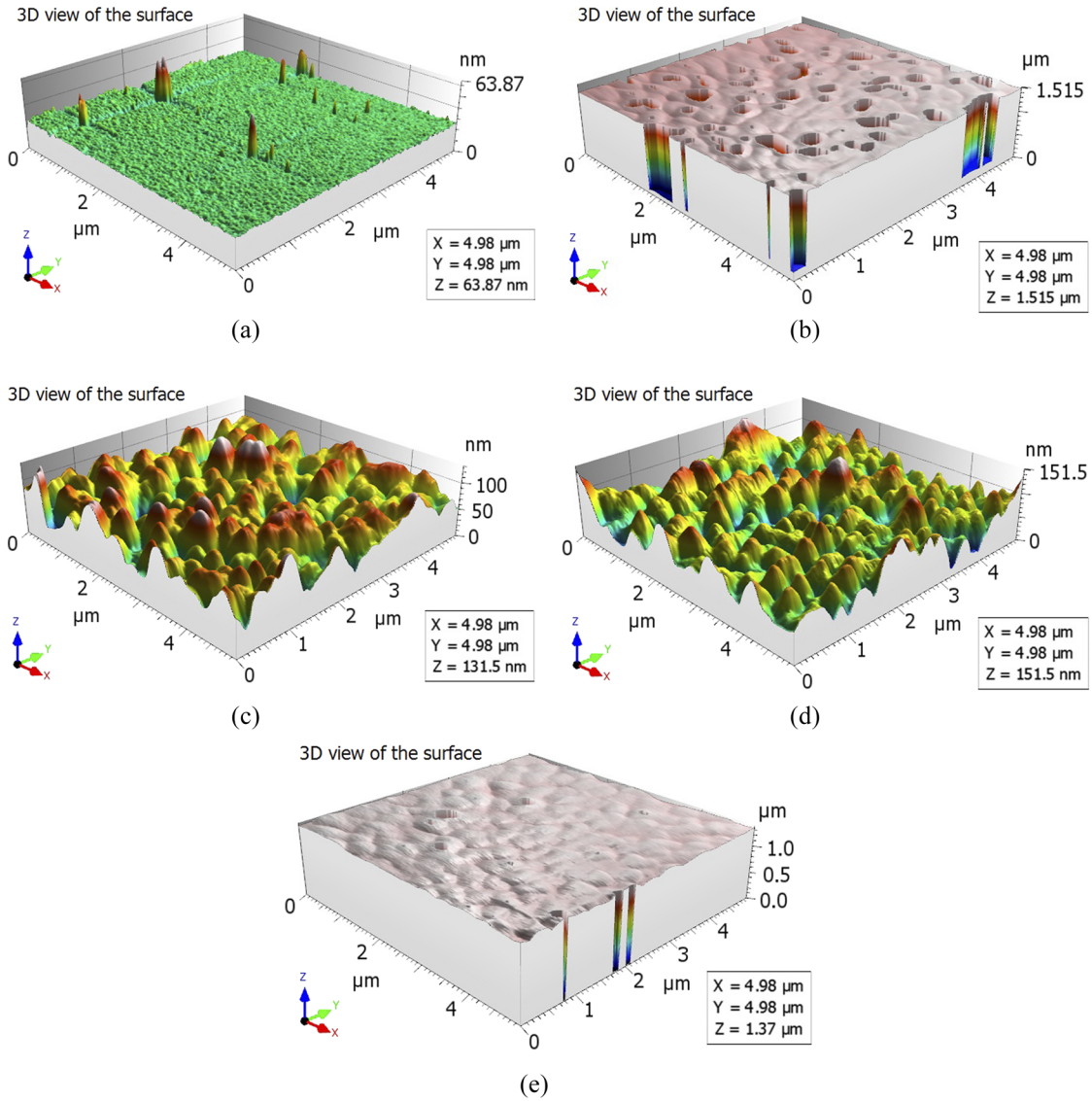

FIG. 3. AFM images of DNC film surfaces for (a) no. 1, (b) no. 2, (c) no. 3, (d) no. 4, and (e) no. 5.

B. Stereometric characterization of 3D surface microtextures

MountainsMap® premium software was used to analyze the surface properties of each DNC sample stereometrically,[29] according to six quantitative parameters [functional, height, hybrid, functional (volume), spatial, and feature parameters] obtained through AFM images and ISO 25178-2: 2012.[30] 3D surface roughness was estimated based on the objective parameters which are reported in Ref. 16. In the present study, fractal geometry and statistical parameters are the two main criteria for 3D surface roughness characterization.

III. RESULTS AND DISCUSSION

Figure 1 indicates Au and Si contents of gold thin films deposited on the Si substrate through RBS analyses. SIMN RA software (SIMNRA by Mayer, 1996) determined the Au film thickness as 90 nm.

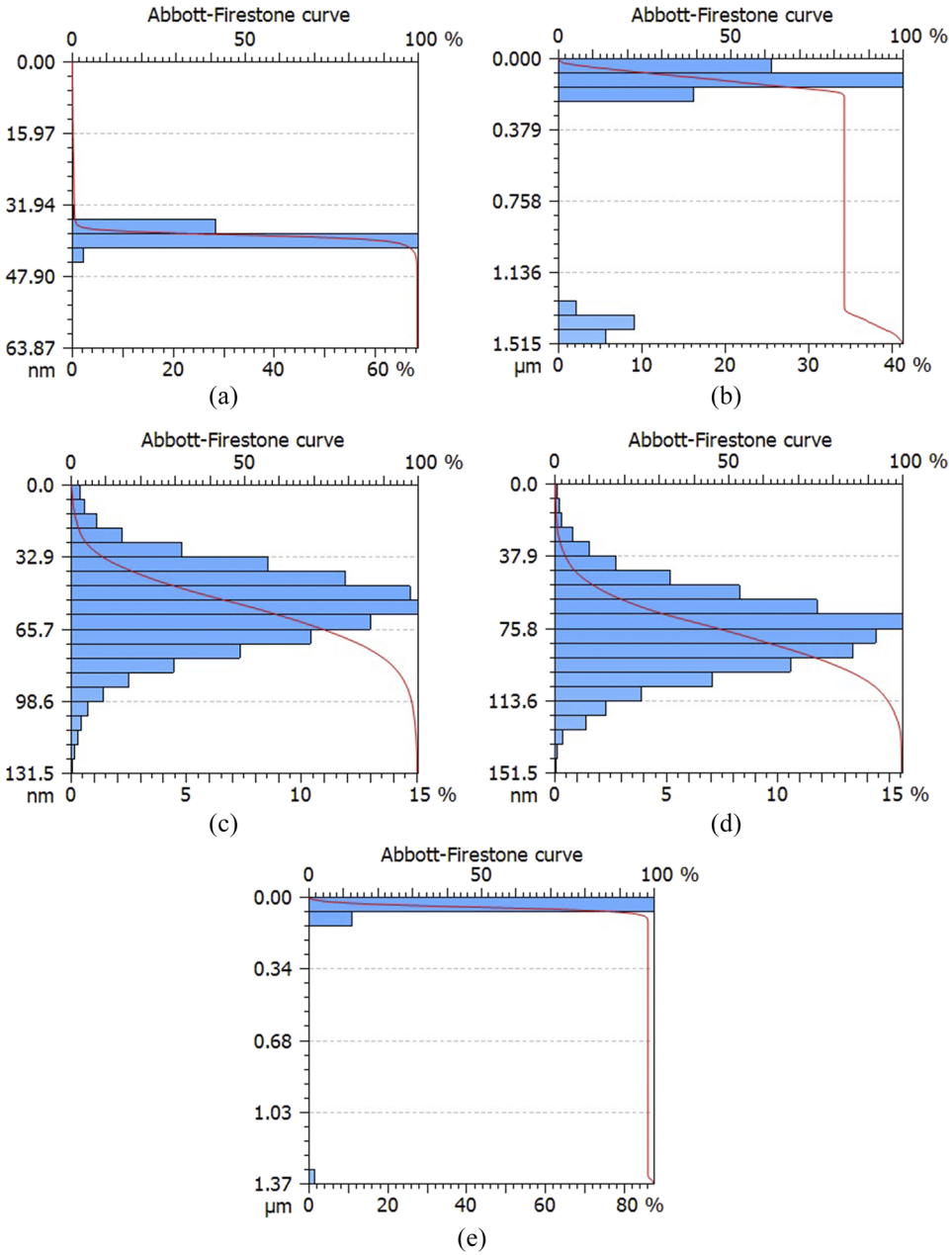

FIG. 4. Depth histograms of the DNC film surfaces for (a) no. 1, (b) no. 2, (c) no. 3, (d) no. 4, and (e) no. 5.

In Fig. 2, the XRD patterns of the DNC films are illustrated for samples grown for 15 min, 30 min, and 60 min. A sharp Au(111) peak at 47° is observable in all samples. However, in sample nos. 4 and 5, with 30 min and 60 min growth, respectively, the existence of C(002) and C(111) peaks at 28° and 43°, respectively, demonstrates the fact that increasing the duration of DNC growth results in better crystalline quality of the samples.

3D AFM images of the surfaces of DNC films are shown in Fig. 3 for 5 × 5 μm^2 scanning square areas: (a) no. 1, (b) no. 2, (c) no. 3, (d) no. 4, and (e) no. 5.

Figure 4 presents the depth histograms, which helps us investigate the distribution density of the data points on the surface. The vertical and horizontal axes indicate the depths and the whole population (%), respectively. The percentage of traversed

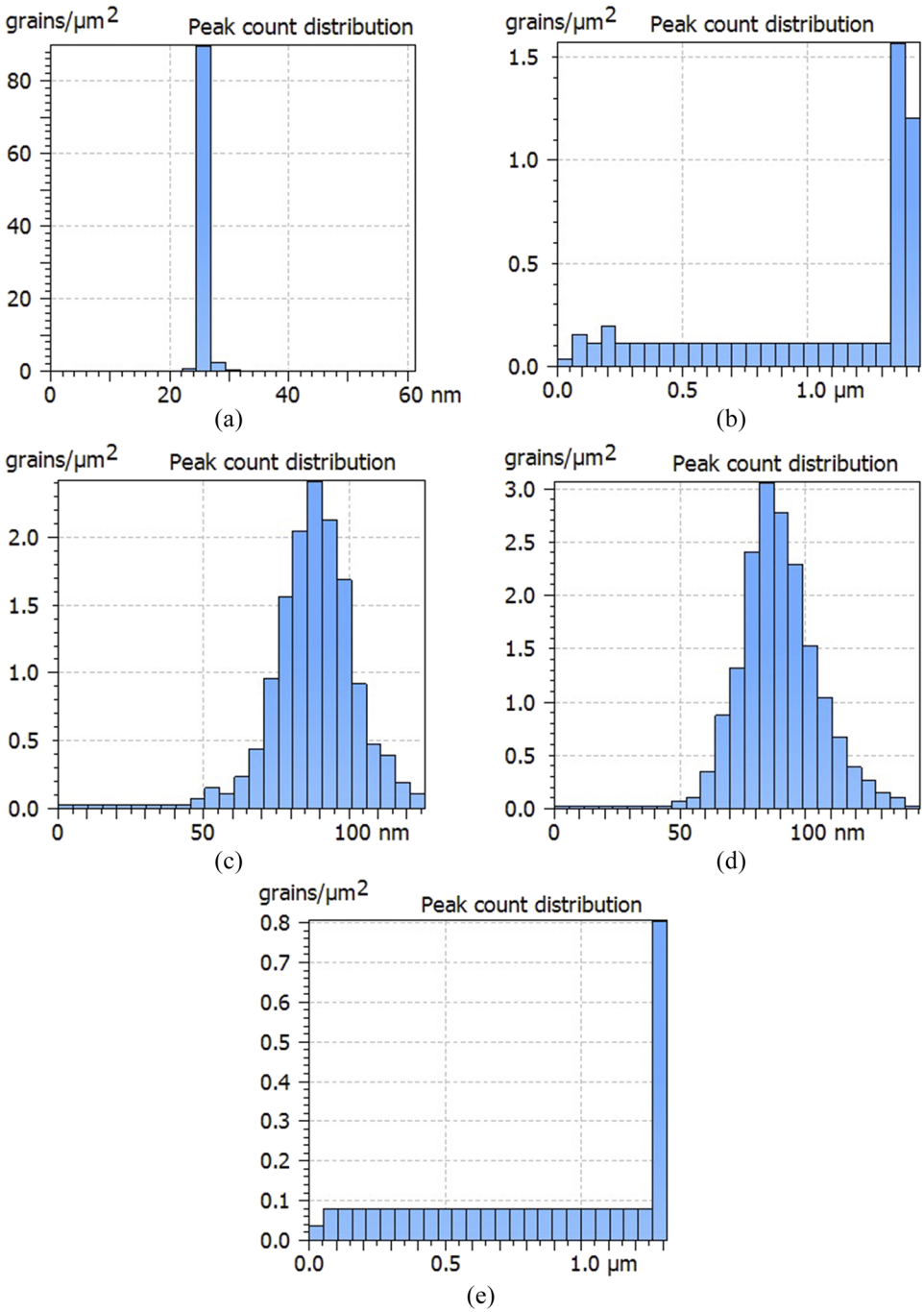

FIG. 5. Peak count histograms for (a) no. 1, (b) no. 2, (c) no. 3, (d) no. 4, and (e) no. 5.

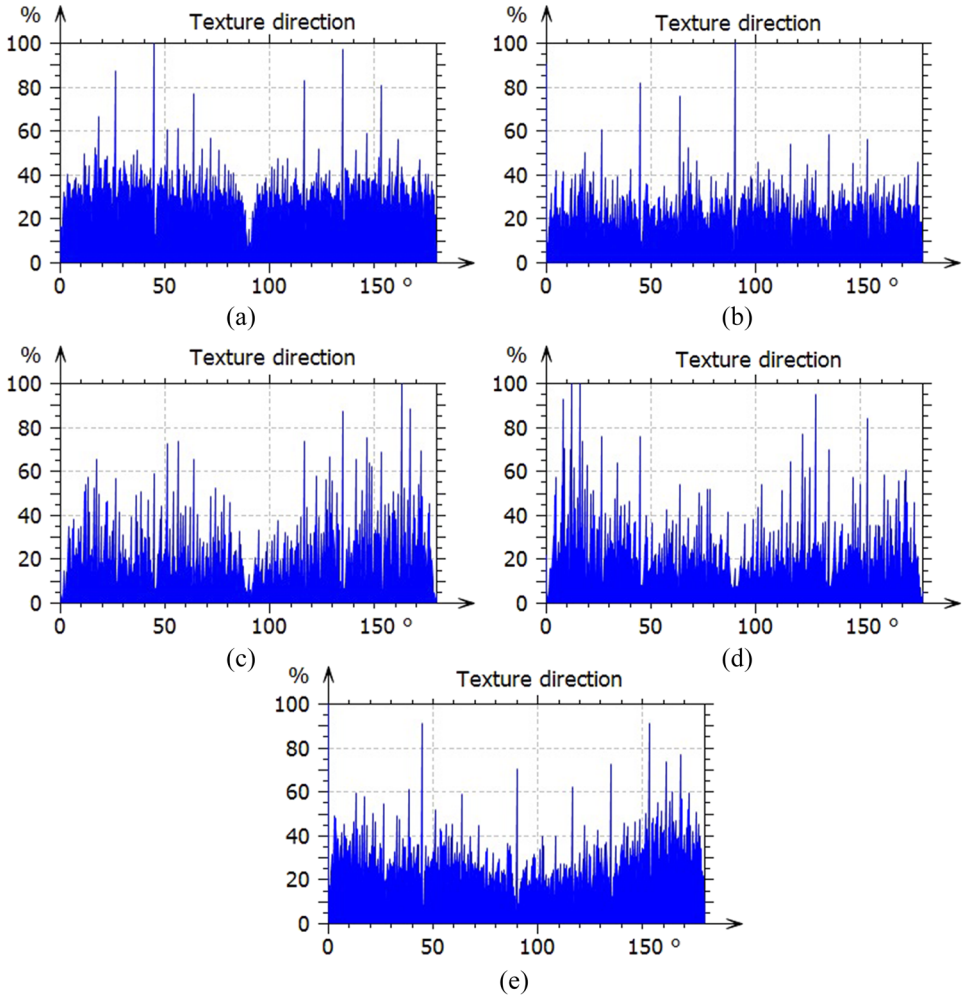

FIG. 6. Texture directions of the sample surfaces using Cartesian graphs for (a) no. 1, (b) no. 2, (c) no. 3, (d) no. 4, and (e) no. 5.

material in relation to the covered area is called the bearing ratio curve, and it is obtained through the Abbott–Firestone curve, which is the cumulative function of amplitude distribution. Here, the horizontal axis also represents the percentage of the bearing ratio.

In addition, the peak count histogram for each sample is shown in Fig. 5.

Cartesian graphs shown in Fig. 6 also represent surface texture directions whose corresponding value for each sample is summarized in Table II.

As can be seen, the highest and lowest values of the isotropy parameter are related to sample no. 2 (82.44%) and sample no. 4 (24.43%), respectively, while other samples have values of about 70%. The maximum value of the first direction

TABLE II. Texture directions of the surfaces of DNC samples shown in Fig. 6.

Sample nos.	Isotropy (%)	First direction (deg)	Second direction (deg)	Third direction (deg)
1	70.60	44.98	135.0	26.46
2	82.44	90.00	0.178	44.99
3	74.83	163.0	135.0	146.3
4	24.43	11.93	128.8	153.5
5	67.68	0.208	153.5	44.99

parameter is observed in sample no. 3 (163°), whereas the minimum value of this parameter was obtained in sample no. 5 (0.208°). For the second direction, however, the maximum and minimum value were related to sample no. 5 (153°) and sample no. 2 (0.178°), respectively. Finally, the highest value of the third direction parameter is achieved in sample no. 4 (153.0°), while the lowest value was achieved in sample no. 1 (26.46°).

Moreover, Table III summarizes all surface texture parameters deduced from 5 × 5 μm^2 scanning square areas of AFM images, according to ISO 25178-2: 2012, whose details are reported in Ref. 16. As can be seen, the lowest and largest root mean heights (Sq) belong to the Au catalyst as sample no. 1 (1.87 nm) and sample no. 3 with (158.9 nm), respectively. Furthermore, by increasing the time of DNC growth from 15 nm to 60 min, Sq is increased,

TABLE III. Statistical parameters of samples: (a) no. 1, (b) no. 2, (c) no. 3, (d) no. 4, and (e) no. 5 with a statistical difference of $P < 0.05$ for all values.

		Scanning square areas of 5 × 5 μm^2				
Statistical parameters	Symbol	No. 1	No. 2	No. 3	No. 4	No. 5
Height Parameters						
Root mean square height	Sq (nm)	1.87	492.9	18.19	20.51	158.9
Skewness	Ssk	8.31	−1.75	−0.241	0.084	−7.86
Kurtosis	Sku	132.3	4.12	3.442	3.227	63.67
Maximum peak height	Sp (nm)	38.76	324.7	55.81	77.72	66.78
Maximum pit height	Sv (nm)	25.11	1 190	75.64	73.80	1303
Maximum height	Sz (nm)	63.87	1 515	131.5	151.5	1370
Arithmetic mean height	Sa (nm)	0.87	367.2	14.25	16.17	40.7
Functional Parameters						
Areal material ratio	Smr (%)	100	83.18	100	100	98.51
Inverse areal material ratio	Smc (nm)	1.07	279.4	22.06	25.80	41.15
Extreme peak height	Sxp (nm)	2.67	1 346	39.06	41.22	42.63
Spatial Parameters						
Auto-correlation length	Sal (μm)	0.083 7	0.150 2	0.262 4	0.244 2	0.134 8
Hybrid Parameters						
Root mean square gradient	Sdq	0.079 8	16.95	0.175 5	0.206 7	6.266
Developed interfacial area ratio	Sdr (%)	0.293 7	378.3	1.498	2.091	53.50
Functional Parameters (Volume)						
Material volume	Vm ($\mu m^3/\mu m^2$)	0.000 146	0.001 337	0.000 858	0.001 1	0.000 775
Void volume	Vv ($\mu m^3/\mu m^2$)	0.001 217	0.280 7	0.022 92	0.026 89	0.041 92
Peak material volume	Vmp ($\mu m^3/\mu m^2$)	0.000 146	0.001 337	0.000 858	0.001 1	0.000 775
Core material volume	Vmc ($\mu m^3/\mu m^2$)	0.000 805	0.058 01	0.016 06	0.018 21	0.015 8
Core void volume	Vvc ($\mu m^3/\mu m^2$)	0.001 041	0.071 76	0.020 62	0.024 6	0.020 8
Pit void volume	Vvv ($\mu m^3/\mu m^2$)	0.000 175	0.209 0	0.002 295	0.002 298	0.021 12
Feature Parameters						
Density of peaks	Spd ($1/\mu m^2$)	1.492	0.120 9	3.104	3.910	0.040 3
Arithmetic mean peak curvature	Spc ($1/\mu m$)	9.839	5 308	2.428	4.017	6.427
Ten-point height	S10z (nm)	50.26	1 312	118.4	127.1	1 214
Five-point peak height	S5p (nm)	32.12	287.2	52.18	66.57	58.32
Five-point pit height	S5v (nm)	18.14	1 185	66.22	60.51	1 301
Mean dales area	Sda (μm^2)	0.539 8	0.094 17	0.564 0	0.343 9	0.030 04
Mean hills area	Sha (μm^2)	0.369 9	0.058 36	0.336 0	0.274 7	0.061 24
Mean dales volume	Sdv (μm^3)	4.27×10^{-5}	0.086 48	0.001 101	4.54×10^{-4}	0.031 45
Mean hills volume	Shv (μm^3)	1.39×10^{-4}	5.39×10^{-4}	0.001 009	9.32×10^{-4}	6.24×10^{-4}
Functional parameters (Stratified surfaces)						
Core roughness depth	Sk (nm)	2.15	186.5	44.0	50.86	43.14
Reduced peak height	Spk (nm)	2.91	15.3	17.09	22.09	15.69
Reduced valley depth	Svk (nm)	1.90	2404	21.56	20.29	331.8
Peak material portion	Smr1 (%)	10.03	2.583	9.294	10.27	10.11
Peak valley portion	Smr2 (%)	86.77	83.17	88.30	89.61	87.94

TABLE IV. The fractal dimensions (*Df*) for analyzed samples. The average results were expressed as standard deviation and mean value. Statistical difference: $P < 0.05$.

Fractal dimension	No. 1	No. 2	No. 3	No. 4	No. 5
Df	2.43 ± 0.01	2.34 ± 0.01	2.17 ± 0.01	2.65 ± 0.01	2.28 ± 0.01

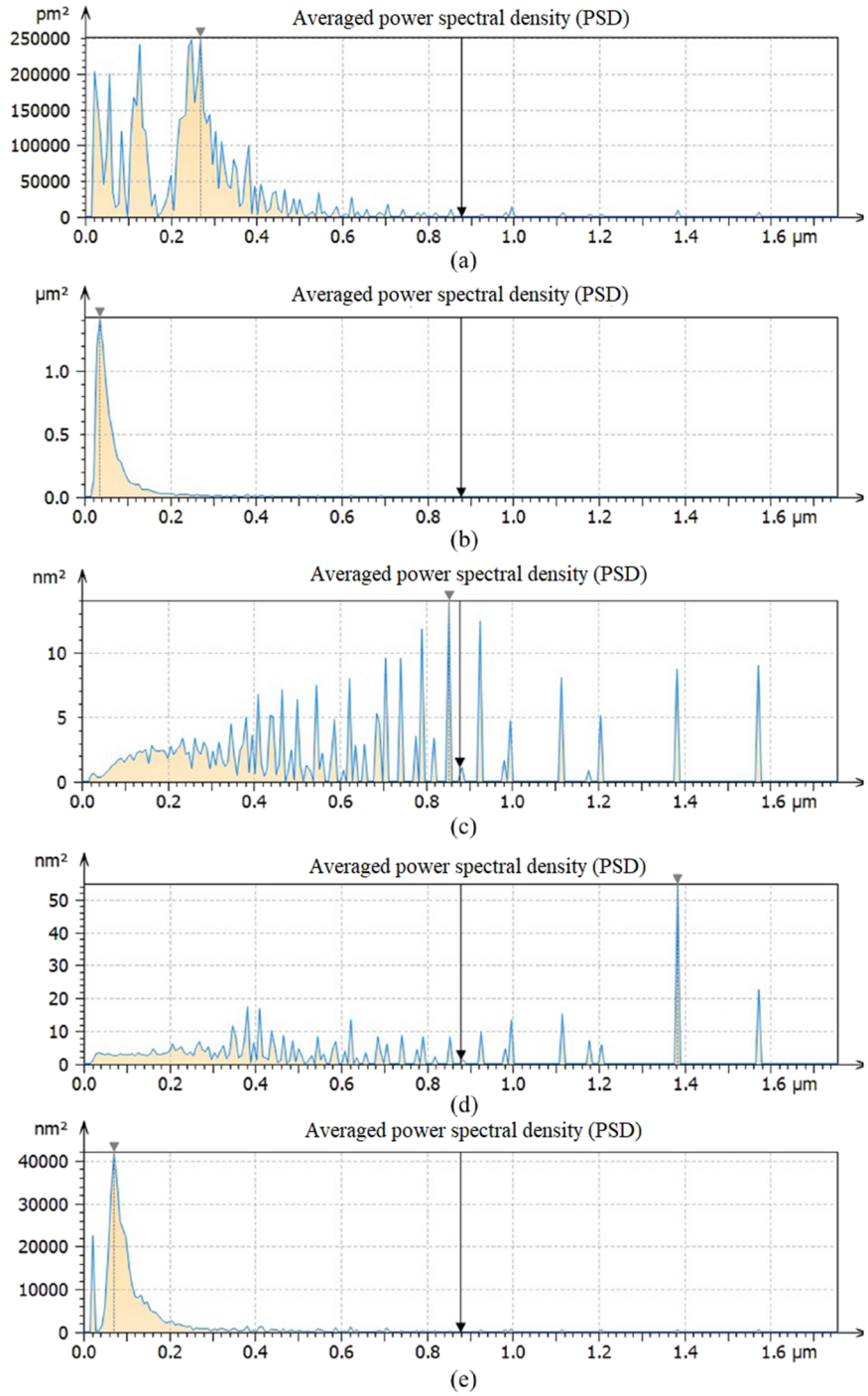

FIG. 7. The average PSD of surface textures for (a) no. 1, (b) no. 2, (c) no. 3, (d) no. 4, and (e) no. 5.

TABLE V. The average PSD parameters for the analyzed samples.

Average PSD parameters	No. 1	No. 2	No. 3	No. 4	No. 5
Wavelength (μm)	0.8813	0.8813	0.8813	0.8813	0.8813
Amplitude (nm)	0.0244	7.516	1.063	1.163	2.849
Dominant wavelength (μm)	0.2679	0.0352	0.8531	1.382	0.0705
Maximum amplitude (nm)	0.5015	1195	3.746	7.403	205.1

TABLE VI. The furrow parameters of samples.

Parameters of furrows	No. 1	No. 2	No. 3	No. 4	No. 5
Maximum depth (nm)	6.209	1539	81.01	71.96	1354
Mean depth (nm)	1.623	483.1	30.48	33.55	123.6
Mean density (cm/cm^2)	52 012	37 427	31 369	34 316	34 821

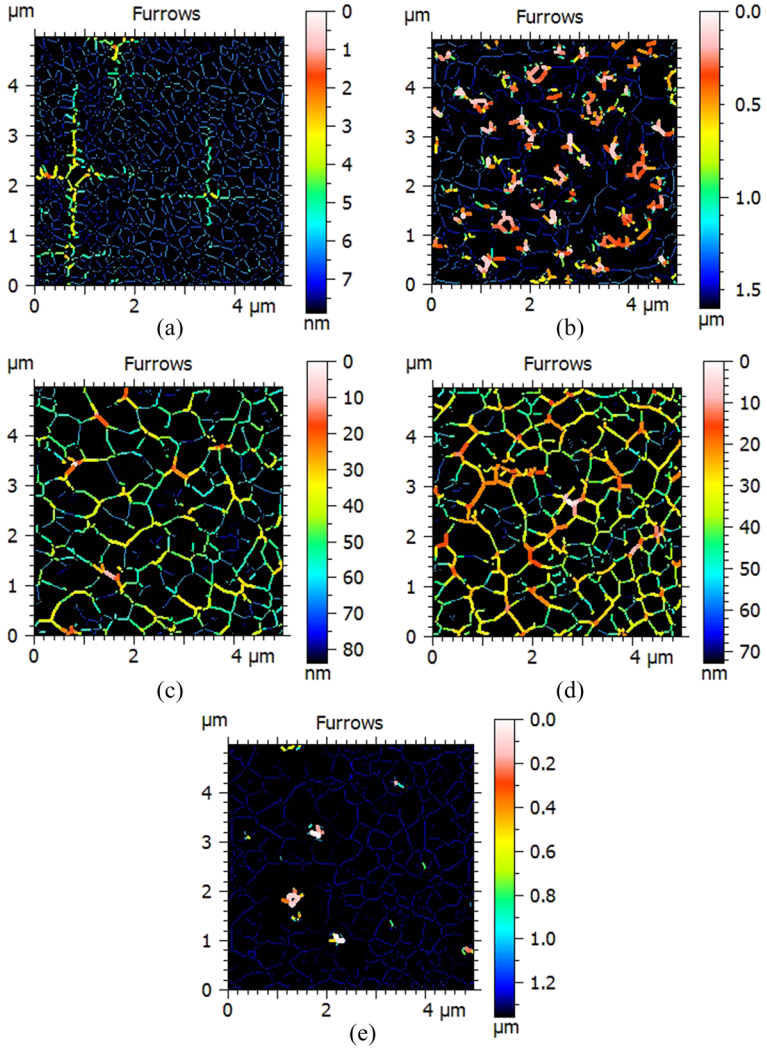

FIG. 8. The furrows of samples for: (a) no. 1, (b) no. 2, (c) no. 3, (d) no. 4, and (e) no. 5.

which indicates an increase in root mean square. The negative value of surface skewness (Ssk) in sample nos. 2, 3, and 5 confirms the dominance of pits on their surfaces, while its positive value in sample nos. 1 and 4 confirms peak dominance.

Surface kurtosis (Sku) is another parameter whose value for all samples is above three and points to the existence of high peaks or valleys on the surface. The maximum and minimum values of Sku are observed in sample nos. 1 (132.3) and 4 (3.227), respectively. In addition, Sv and Sp are the maximum valley depth and maximum peak height, with the maximum value in sample no. 5 (1303 nm) and sample no. 2 (324.7 nm), respectively, and their variation is not non-monotic. Meanwhile, Sz is defined as the sum of the maximum pit height and the maximum peak height, with the greatest value in sample no. 2. In addition, it can be seen that by increasing the time of DNC growth, Sz has increased. The same routine is observable for the arithmetic mean height (Sa), which is the mean of the vertical deviations from the mean surface, and also for S10z, whose values are increased by increasing the time of DNC growth. The maximum value of S10z is obtained in sample no. 2 (1312 nm).

Here, fractal dimensions were calculated by the enclosing boxes method with coefficients of correlation (R^2) and are summarized in Table IV. As can be seen, the values of R^2 for all linear fits were 0.998 ± 0.001, which confirm the excellent data fit by linear functions.

On the other hand, the average power spectral density (PSD) of surface textures is shown in Fig. 7, and its values are summarized in Table V.

The furrows of samples (including mean depth of furrows and mean density of furrows along with the maximum depth of furrows specified in Table VI) are shown in Fig. 8.

IV. CONCLUSIONS

We mainly focused on the synthesis of DNC thin films on a Si substrate in the present approach and then used AFM and multifractal analysis to investigate their morphological features. In this aim, an Au catalyst was applied, and DNC growth was carried out by the HFCVD method for different durations: 15 min, 30 min, and 60 min.

The 3D surface microtexture characteristics of DNC thin films were quantitatively investigated by the Abbott–Firestone curve and fractal geometry along with other stereometric analyses such as furrows and average PSD. According to these parameters, microstructures and surface texture will be investigated with high precision and easy implementation. According to the results of the present study, a new insight into diamond nanocrystallines can be achieved in the field of thin film morphology. Studying these statistical parameters demonstrated that among the prepared specimens, sample no. 2, which was the Au etched thin film produced by the HFCVD method, was the most isotropic sample with the maximum surface roughness (492.9 nm). Moreover, by increasing the DNC growth duration, surface roughness was increased, and the surface became irregular. In addition, the most regular topography (Df = 2.17 ± 0.01) was found in sample no. 3, while the most irregular topography (Df = 2.65 ± 0.01) was found in sample no. 4.

ACKNOWLEDGMENTS

The authors report no conflict of interests. The authors alone are responsible for the content and writing of the paper.

REFERENCES

[1] A. Mahmoodi, S. Solaymani, M. Amini, N. B. Nezafat, M. Ghoranneviss, "Structural, Morphological and antibacterial characterization of CuO nanowires," Silicon **10**, 1427 (2018).
[2] D. Zhou, T. G. McCauley, L. C. Qin, A. R. Krauss, and D. M. Gruen, "Synthesis of nanocrystalline diamond thin films from an Ar–CH_4 microwave plasma," J. Appl. Phys. **83**, 540 (1998).
[3] S. Majidi, N. B. Nezafat, D. P. Rai, A. Achour, H. Ghaziasadi, and A. Sheykhian, "Optical and electronic properties of pure and fully hydrogenated SiC and GeC nanosheets: First-principles study," Opt. Quantum Electron. **50**, 292 (2018).
[4] Ş. Ţălu, R. P. Yadav, T. Lainović, A. Méndez-Albores, G. Trejo, D. Kukuruzović, N. B. Nezafat, A. Shafiekhani, and Sh. Solaymani, "The effect of dental LED light-curing unit photoactivation mode on 3D surface morphology of dental nanocomposites evaluated by two-dimensional multifractal detrended fluctuation analysis," Microsc. Res. Tech. **81**(10), 1223–1230 (2018).
[5] J. R. Rabeau, A. Stacey, A. Rabeau, S. Prawer, F. Jelezko, I. Mirza, and J. Wrachtrup, "Single nitrogen vacancy centers in chemical vapor deposited diamond nanocrystals," Nano Lett. **7**(11), 3433–3437 (2007).
[6] H. Li, H.-J. Lee, J.-K. Park, Y.-J. Baik, G. W. Hwang, J.-h. Jeong, and W.-S. Lee, "Control of abnormal grain inclusions in the nanocrystalline diamond film deposited by hot filament CVD," Diamond. Relat. Mater. **18**(11), 1369–1374 (2009).
[7] J. Birrell, J. E. Gerbi, O. Auciello, J. M. Gibson, J. Johnson, and J. A. Carlisle, "Interpretation of the Raman spectra of ultrananocrystalline diamond," Diamond. Relat. Mater. **14**(1), 86–92 (2005).
[8] J. R. Maze, P. L. Stanwix, J. S. Hodges *et al.*, "Nanoscale magnetic sensing with an individual electronic spin in diamond," Nature **455**, 644–647 (2008).
[9] S. Solaymani, A. Ghaderi, and N. B. Nezafat, "Comment on: "Characterization of microroughness parameters in titanium nitride thin films grown by DC magnetron sputtering"," J. Fusion Energy **31**, 591 (2012).
[10] S. Solaymani, S. M. Elahi, N. B. Nezafat, H. Zahrabi, A. Boochani, and M. Naseri, "Characterization of microroughness parameters in Cu–C nanocomposite prepared by co-deposition of RF-sputtering and RF-PECVD," Eur. Phys. J. Appl. Phys. **64**, 11301 (2013).
[11] Ş. Ţălu, M. Bramowicz, S. Kulesza, A. Ghaderi, V. Dalouji, S. Solaymani, M. F. Kenari, and M. Ghoranneviss, "Fractal features and surface micromorphology of diamond nanocrystals," J. Microsc. **264**(2), 143–152 (2016).
[12] M. T. Dikonimos, R. Giorgi, N. Lisi, L. Pilloni, and E. Salernitano, "Bias enhanced nucleation of diamond on Si(100) in a vertical straight hot filament CVD," Diamond. Relat. Mater. **14**, 318–322 (2005).
[13] D. M. Gruen, A. R. Krauss, D. Zhou, T. G. McCauley, T. D. Corrigan, R. P. H. Chang, and G. M. Swain, in *The Electrochemical Society Proceedings* (The Electrochemical Society, Pennington, NJ, 1997), Vol. 97-25, p. 325.
[14] S. A. Catlegde and Y. K. Vohra, "Structure and stress evaluation of diamond films deposited on Ti-6A1-4V alloy at low temperature using $CH_4/O_2/H_2$ and CO/H_2 gas mixtures," Mater. Res. Soc. Symp. Proc. **505**, 629 (1997).
[15] S. A. Catlegde and Y. K. Vohra, "*In situ* diagnostics of film thickness and surface roughness of diamond films on a Ti–6Al–4V alloy by optical pyrometry," J. Appl. Phys. Lett. **73**, 181 (1998).
[16] Ş. Ţălu, *Micro and Nanoscale Characterization of Three Dimensional Surfaces. Basics and Applications* (Napoca Star Publishing House, Cluj-Napoca, Romania, 2015).
[17] N. B. Nezafat, M. Ghoranneviss, S. M. Elahi, A. Shafiekhani, Z. Ghorannevis, and S. Solaymani, "Topographic characterization of canine teeth using atomic force microscopy images in nano-scale," Int. Nano Lett. **9**, 311 (2019).
[18] A. Roudbari, V. Dalouji, S. Solaymani, N. B. Nezafat, and S. Rezaee, "The effect of geometry characterizations and annealing processing on dissipation electrical energy in ZnO films," Int. J. Thermophys. **40**(8), 75 (2019).
[19] N. B. Nezafat, M. Ghoranneviss, S. M. Elahi, A. Shafiekhani, Z. Ghorannevis, and S. Solaymani, "Microstructure, micromorphology, and fractal geometry of hard dental tissues: Evaluation of atomic force microscopy images," Microsc. Res. Tech. **82**(11), 1884–1890 (2019).

[20]R. P. Yadav, S. Dwivedi, A. K. Mittal, M. Kumar, and A. C. Pandey, "Fractal and multifractal analysis of LiF thin film surface," Appl. Surf. Sci. **261**, 547–553 (2012).
[21]Ş. Ţălu, M. Bramowicz, S. Kulesza, A. Shafiekhani, A. Ghaderi, F. Mashayekhi, and S. Solaymani, "Microstructure and tribological properties of FeNPs@a-C:H films by micromorphology analysis and fractal geometry," Ind. Eng. Chem. Res. **54**(33), 8212–8218 (2015).
[22]Ş. Ţălu, S. Stach, A. Mahajan, D. Pathak, T. Wagner, A. Kumar, and R. K. Bedi, "Multifractal analysis of drop-casted copper(II) tetrasulfophthalocyanine film surfaces on the indium tin oxide substrates," Surf. Interface Anal. **46**(6), 393–398 (2014).
[23]Ş. Ţălu, S. Stach, S. Solaymani, R. Moradian, A. Ghaderi, M. R. Hantehzadeh, S. M. Elahi, Ż. Garczyk, and S. Izadyar, "Multifractal spectra of atomic force microscope images of Cu/Fe nanoparticles based films thickness," J. Electroanal. Chem. **79**, 31–41 (2015).
[24]N. Naseri, S. Solaymani, A. Ghaderi, M. Bramowicz, S. Kulesza, Ş. Ţălu, M. Pourreza, and S. Ghasemi, "Microstructure, morphology and electrochemical properties of Co nanoflake water oxidation electrocatalyst at micro- and nanoscale," RSC Adv. **7**(21), 12923–12930 (2017).
[25]D. Sobola, Ş. Ţălu, S. Solaymani, and L. Grmela, "Influence of scanning rate on quality of AFM image: Study of surface statistical metrics," Microsc. Res. Tech. **80**(12), 1328–1336 (2017).
[26]M. Zare, S. Solaymani, A. Shafiekhani, S. Kulesza, Ş. Ţălu, and M. Bramowicz, "Evolution of rough-surface geometry and crystalline structures of aligned TiO_2 nanotubes for photoelectrochemical water splitting," Sci. Rep. **8**, 10870 (2018).
[27]P. Azadfar, M. Ghoranneviss, S. M. Elahi, N. Farhadyar, and A. Salar Elahi, "Growth of boron-doped diamond nanoclusters using the HFCVD technique," J. Cryst. Growth **415**, 166–169 (2015).
[28]CSM Instruments, "Overview of mechanical testing standards," in *Applications Bulletin*, edited by N. Randall (CSM Instruments, Peseux, Switzerland, 2002), Vol. 18.
[29]Mountains Map® 8 premium Software (Digital Surf, Besançon, France), available from: http://www.digitalsurf.fr; accessed 14 December 2019.
[30]ISO 25178-2: 2012, Geometrical product specifications (GPS), Surface texture: Areal, Part 2: Terms, definitions and surface texture parameters, available from: http://www.iso.org; accessed on 14 December 2019.